



Polar mesospheric clouds observed by Himawari-8

Takuo T. Tsuda¹, Yuta Hozumi¹, Kento Kawaura¹, Keisuke Hosokawa¹, Hidehiko Suzuki², and Takuji Nakamura^{3,4}

¹Department of Computer and Network Engineering, The University of Electro-Communications, Chofu, Japan.

²Department of Physics, Meiji University, Kawasaki, Japan.

³National Institute of Polar Research (NIPR), Tachikawa, Japan.

⁴Department of Polar Science, Graduate University for Advanced Studies (SOKENDAI), Tachikawa, Japan.

Correspondence: Takuo T. Tsuda (takuo.tsuda@uec.ac.jp)

Abstract. We make an initial report on polar mesospheric clouds (PMCs) observed by Himawari-8, the Japanese Geostationary-Earth-Orbit (GEO) meteorological satellite. Heights of the observed PMCs were estimated to be 80–82 km. The PMCs were active only during summertime in both the northern and southern polar regions. These results are concrete evidences of PMCs. PMC observations by Himawari-8 can provide continuous PMC monitoring at every 10 minutes with 3 visible bands from its almost fixed location relative to the Earth, and it would enhance PMC research in the near future.

1 Introduction

Polar mesospheric clouds (PMCs) or noctilucent clouds (NLCs) consist of water-ice particles, which can be produced at cold summer mesopause region, mainly at high latitudes. The first report on PMCs was made by Leslie (1885). Since then, PMC observations have been widely performed by various methods from the ground as well as from the space. Optical observations by ground-based cameras, imagers or lidars are often limited by weather conditions, because the clear sky is required for such observations. Hence, satellite observations from the space are valuable for more continuous observations, which enable more systematic data coverage. Such systematic data coverage would be of benefit, for example, to monitor long-term PMC activities, which may be related with the global change (cf. Thomas, 1996; von Zahn, 2003) because mesosphere cooling, which can enhance water-ice particle production, may be induced by CO₂ and CH₄ increases (cf. Roble and Dickinson, 1989).

A comprehensive review in PMC observations from satellites can be found in DeLand et al. (2006). In addition, Aeronomy of Ice in the Mesosphere (AIM) satellite has been in operation for PMC observations since 2007 (Russell et al., 2009). These observations include both limb- and nadir-viewing from low-Earth-orbit (LEO) satellites. On the other hand, there are only a few reports on PMC observations by limb-viewing from Geostationary-Earth-Orbit (GEO) satellites (Gadsden, 2000a, b, 2001; Proud, 2015). The first PMC observations from GEO were reported using images by Meteosat First Generation (MFG) (Gadsden, 2000a, b, 2001), and their PMC images had ~2.5-km spatial resolution in a single visible band. Then, Proud (2015) extended such observations to Meteosat Second Generation (MSG), and they reported PMC observations using ~1-km spatial resolution images in a single visible band. This kind of GEO satellite can produce full-disk images including the Earth's limb,



which would provide valuable opportunities for PMC observations by continuous limb-viewing from its almost fixed locations relative to the Earth.

In the present paper, we make an initial report on PMC observations from Himawari-8, the Japanese GEO meteorological satellite. Our PMC images by Himawari-8 have ~ 1 -km spatial resolution in 3 visible bands. The Japanese GEO meteorological satellites have a long history from 1977 (Himawari-1) to the present (Himawari-8). However, there was no PMC report from the Japanese GEO satellite observations before this work. For this reason, in the present paper we examine basic features in PMC emissions observed by Himawari-8 and compare those with typical PMC characteristics, as a first step for our PMC research using Himawari-8 data.

10

2 Data

Himawari-8 is the Japanese GEO meteorological satellite (Bessho et al., 2016), which was successfully launched in October 2014. Himawari-8 has 16 observation bands including 3 visible bands, blue ($0.47 \mu\text{m}$), green ($0.51 \mu\text{m}$), and red ($0.64 \mu\text{m}$). In the initial survey for PMCs, we used full-disk images in Portable Network Graphics (PNG) format, which are generated from the level-1a data, Himawari Standard Data (HSD). The PNG full disk image is a true-color image (composites of the 3 visible bands). Each color has 8-bit resolution (i.e., 0 to 255 counts), which describes emission intensities from 0 to $641.5092 \text{ W m}^{-2} \text{ sr}^{-1} \mu\text{m}^{-1}$ for the blue band, from 0 to $601.9766 \text{ W m}^{-2} \text{ sr}^{-1} \mu\text{m}^{-1}$ for the green band, and from 0 to $519.3457 \text{ W m}^{-2} \text{ sr}^{-1} \mu\text{m}^{-1}$ for the red band. The PNG full-disk image has the spatial resolution of $\sim 1 \text{ km}$ and is obtained every 10 minutes. More detailed information for the PNG images can be found in Bessho et al. (2016). For the present survey, we collected one-year PNG images in 2016, and focused our attention on the Earth's limb region which corresponds to the outside of the spherical Earth (i.e., the middle and upper atmospheric region).

15
20

3 Results and discussion

Figure 1 shows an example of PMC emissions observed at 21:00 UT on 9 July 2016 in the northern high latitudes. It is difficult to see any emissions in the limb region in the original true-color image (Figure 1a), but it is obvious that clear emissions exist in the limb region in the 50 times-enhanced image (Figure 1b). The appearance of emissions are very similar to those of PMC emissions in the previous reports (Gadsden, 2000a, b, 2001; Proud, 2015). We calculated heights and latitudes of tangential points in each line-of-sight (LOS) direction (i.e., for each pixel in the image). The heights and latitudes of tangential points are overlaid in Figure 1c. As shown in Figure 1c, the height of the emissions was roughly 80 km.

25
30



To see in more detail, height-latitude distributions of the emission intensities in the 3 visible bands are shown in Figure 2. The emissions were mainly located at 80–82 km height in 78–81°N. The emission height (80–82 km) is well consistent with the typical PMC heights (82–83 km) (cf. DeLand et al., 2006). In addition, it seems that the emissions had some fine structures, which were probably due to atmospheric waves, in the height-latitude cross-section. Such fine PMC structures in the height-
5 latitude cross-section would be valuable, because it would be difficult to obtain this kind information by LEO satellites.

The emission intensity in the blue band was the strongest, and that in the red band was the weakest. This may be reasonable if we consider the Mie scattering of sunlight by water-ice particles (i.e., PMCs). The Mie scattering can be effective when the particle size reaches roughly one tenth the wavelength. Hence, smaller particles would induce sunlight scattering only in
10 shorter wavelengths, while larger particles would induce sunlight scattering for both shorter and longer wavelengths. Thus, sunlight scattering (i.e., emission intensity) at shorter wavelengths could be stronger. This would imply that 3 visible images obtained by Himawari-8 may be able to provide useful information on the size of water-ice particles, and it would be one of the future works.

We calculated total counts (i.e., total emission intensities) in specific regions to investigate seasonal variations of the PMC
15 emissions in 2016. We set two regions; one is a region at heights of 70–90 km and latitudes of 60–90°N for northern polar region (Figure 3a), the other is a region at heights of 70–90 km and latitudes of 60–90°S for southern polar region (Figure 3b). The height range of 70–90 km can cover typical PMC occurrence heights, and the latitude range of 60–90° can cover typical PMC occurrence latitudes. It should be noted that the upper limit of the latitude range is actually $\sim 81^\circ$, that is the
20 highest latitude of the tangential points when we set the height range of 70–90 km. The seasonal variations in the total counts are shown in Figure 3, which was from only data at single local time, 06:00 JST (21:00 UT) to remove daily variations. At the local time, 06:00 JST, the LOS of Himawari-8 is almost perpendicular to the sunward direction. This configuration would be beneficial, providing solar illumination to some extent and minimizing sun-induced noise (cf. Proud, 2015). As shown in Figures 3a and 3b, the PMC emissions were active only during local summer months. This is well consistent with the typical
25 PMC active periods (i.e., summertime) (cf. DeLand et al., 2006).

As mentioned above, the heights and seasonal variations of the PMC emissions are well consistent with the general characteristics of PMCs. These results are concrete evidences that the peculiar emissions observed by Himawari-8 are indeed PMCs. Thus, new PMC data obtained from Himawari-8 are introduced. As an advantage of Himawari-8, we suggest that images with
30 the 3 visible bands are available. This may provide valuable opportunities, for example, to obtain information on the size of water-ice particles, because the Mie scattering depends on the relationships between the particle size and the wavelength. In addition, collaborations between Himawari-8 and LEO satellites such as the AIM satellite would be complementary. Especially, high-time resolution data from Himawari-8 (10-minutes resolution), combined with those by LEO satellites, would largely enhance PMC research such as diurnal PMC variations in the near future.



4 Summary

In this paper, we introduced new PMC observations by Himawari-8. The results in the PMC height and the seasonal PMC activity are well consistent with the previously reported PMC characteristics (cf. DeLand et al., 2006). These are not new scientific findings, but these are essentially important for validation of the PMC emissions obtained from new Himawari-8 data. Thus, we demonstrated that Himawari-8 is definitely capable of PMC observations. Himawari-8 can provide new PMC data, and it would enhance valuable opportunities for new PMC research in the near future. Especially, Himawari-8 PMC observations would have following advantages: (1) high-time resolution (10-min); (2) high-spatial resolution (~ 1 -km) in the height-latitude (or height-horizon) cross-section; (3) 3 visible bands, blue ($0.47 \mu\text{m}$), green ($0.51 \mu\text{m}$), and red ($0.64 \mu\text{m}$); (4) continuous monitoring from its almost fixed location relative to the Earth.

10

Data availability. The Himawari-8 data, provided by the Meteorological Satellite Center of the Japan Meteorological Agency (JMA), are available from the National Institute of Information and Communications Technology (NICT) Science Cloud.

Competing interests. The authors declare that they have no conflict of interest.

Acknowledgements. The authors are deeply grateful to Mr. Ryota Yamamoto for providing information on PMC emissions in full-disk images from Himawari-8, and it triggered this work. The Himawari-8 data are provided by the Meteorological Satellite Center of the Japan Meteorological Agency (JMA) through the National Institute of Information and Communications Technology (NICT) Science Cloud. This work was supported in part by MEXT/JSPS KAKENHI Grants, JP15H05815, JP16H01171, JP16H06021, and JP17H02968, by National Institute of Polar Research (NIPR) through General Collaboration Project, no. 28-2, and by the joint research program of the Institute for Space-Earth Environmental Research (ISEE), Nagoya University.



References

- Bessho, K., K. Date, M. Hayashi, A. Ikeda, T. Imai, H. Inoue, Y. Kumagai, T. Miyakawa, H. Murata, T. Ohno, A. Okuyama, R. Oyama, Y. Sasaki, Y. Shimazu, K. Shimoji, and Y. Sumida: An introduction to Himawari-8/9 – Japan’s new-generation geostationary meteorological satellites, *J. Meteorol. Soc. Jpn.*, 94, 151–183, <https://doi.org/10.2151/jmsj.2016-009>, 2016.
- 5 DeLand, M. T., E. P. Shettle, G. E. Thomas, and J. J. Olivero: A quarter-century of satellite polar mesospheric cloud observations, *J. Atmos. Sol. Terr. Phys.*, 68, 9–29, <https://doi.org/10.1016/j.jastp.2005.08.003>, 2006.
- Gadsden, M.: Polar mesospheric clouds seen from geostationary orbit, *J. Atmos. Sol. Terr. Phys.*, 62, 31–36, [https://doi.org/10.1016/S1364-6826\(99\)00099-1](https://doi.org/10.1016/S1364-6826(99)00099-1), 2000a.
- Gadsden, M.: Structure in polar mesospheric clouds seen from a geostationary spacecraft, *Geophys. Res. Lett.*, 27, 3671–3673, <https://doi.org/10.1029/1999GL003682>, 2000b.
- 10 Gadsden, M.: Structure of polar mesospheric clouds seen from a geostationary satellite, *Adv. Space Res.*, 27, 1697–1702, [https://doi.org/10.1016/S0273-1177\(01\)00237-X](https://doi.org/10.1016/S0273-1177(01)00237-X), 2001.
- Leslie, R. C.: Sky glows, *Nature*, 33, 245, <https://doi.org/10.1038/032245a0>, 1885.
- Roble, R. G., and R. E. Dickinson: How will changes in carbon dioxide and methane modify the mean structure of the mesosphere and thermosphere?, *Geophys. Res. Lett.*, 16, 1441–1444, <https://doi.org/10.1029/GL016i012p01441>, 1989.
- 15 Russell, J. M. III, S. M. Bailey, L. L. Gordley, D. W. Rusch, M. Horányi, M. E. Hervig, G. E. Thomas, C. E. Randall, D. E. Siskind, M. H. Stevens, M. E. Summers, M. J. Taylor, C. R. Englert, P. J. Espy, W. E. McClintock, and A. W. Merkel: The Aeronomy of Ice in the Mesosphere (AIM) mission: Overview and early science results, *J. Atmos. Sol. Terr. Phys.*, 71, 289–299, <https://doi.org/10.1016/j.jastp.2008.08.011>, 2009.
- 20 Proud, S.: Observation of polar mesospheric clouds by geostationary satellite sensors, *IEEE Geosci. Remote Sens. Lett.*, 12, 1332–1336, <https://doi.org/10.1109/LGRS.2015.2399532>, 2015.
- Thomas, G. E.: Is the polar mesosphere the miner’s canary of global change?, *Adv. Space Res.*, 18, 149–158, [https://doi.org/10.1016/0273-1177\(95\)00855-9](https://doi.org/10.1016/0273-1177(95)00855-9), 1996.
- 25 von Zahn, U.: Are noctilucent clouds a “Miner’s Canary” for global change?, *Eos Trans. AGU*, 84, 261–264, <https://doi.org/10.1029/2003EO280001>, 2003.

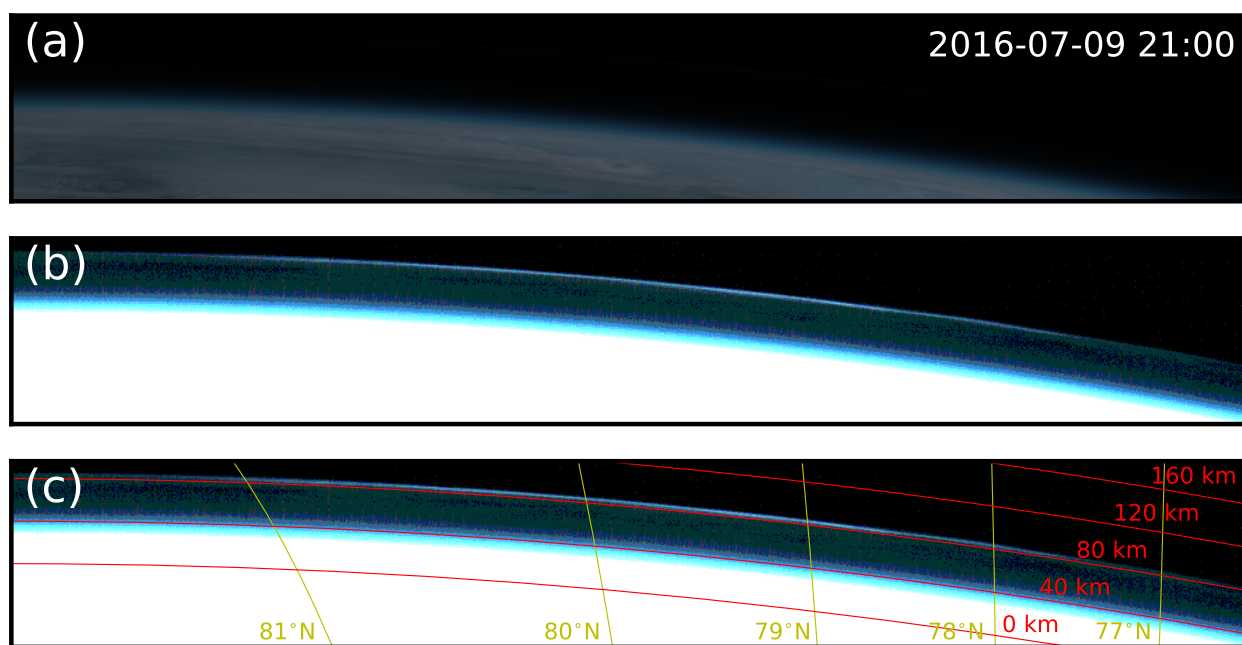


Figure 1. (a) An original true-color image (composites of the 3 visible bands) around northern high latitudes at 21:00 UT on 9 July 2016. (b) Same as Figure 1a, but the color scale is 50 times enhanced. (c) Same as Figure 1b, but latitudes and heights of the tangential points are overlaid.

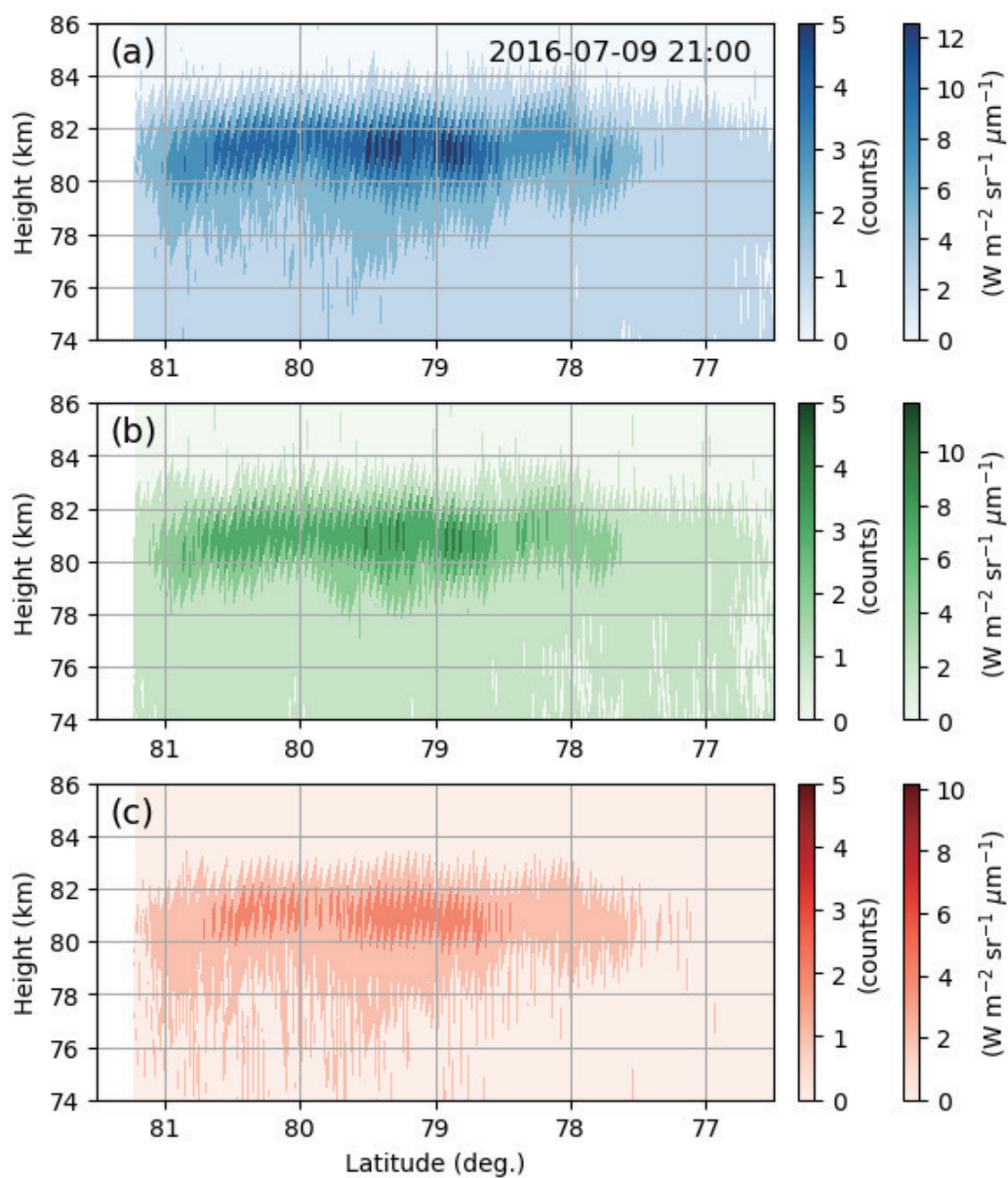


Figure 2. (a) High-latitude distribution of the emission intensity in the blue band on 21:00 UT on 9 July 2016. (b) Same as Figure 2a, but in the green band. (c) Same as Figure 2a, but in the red band.

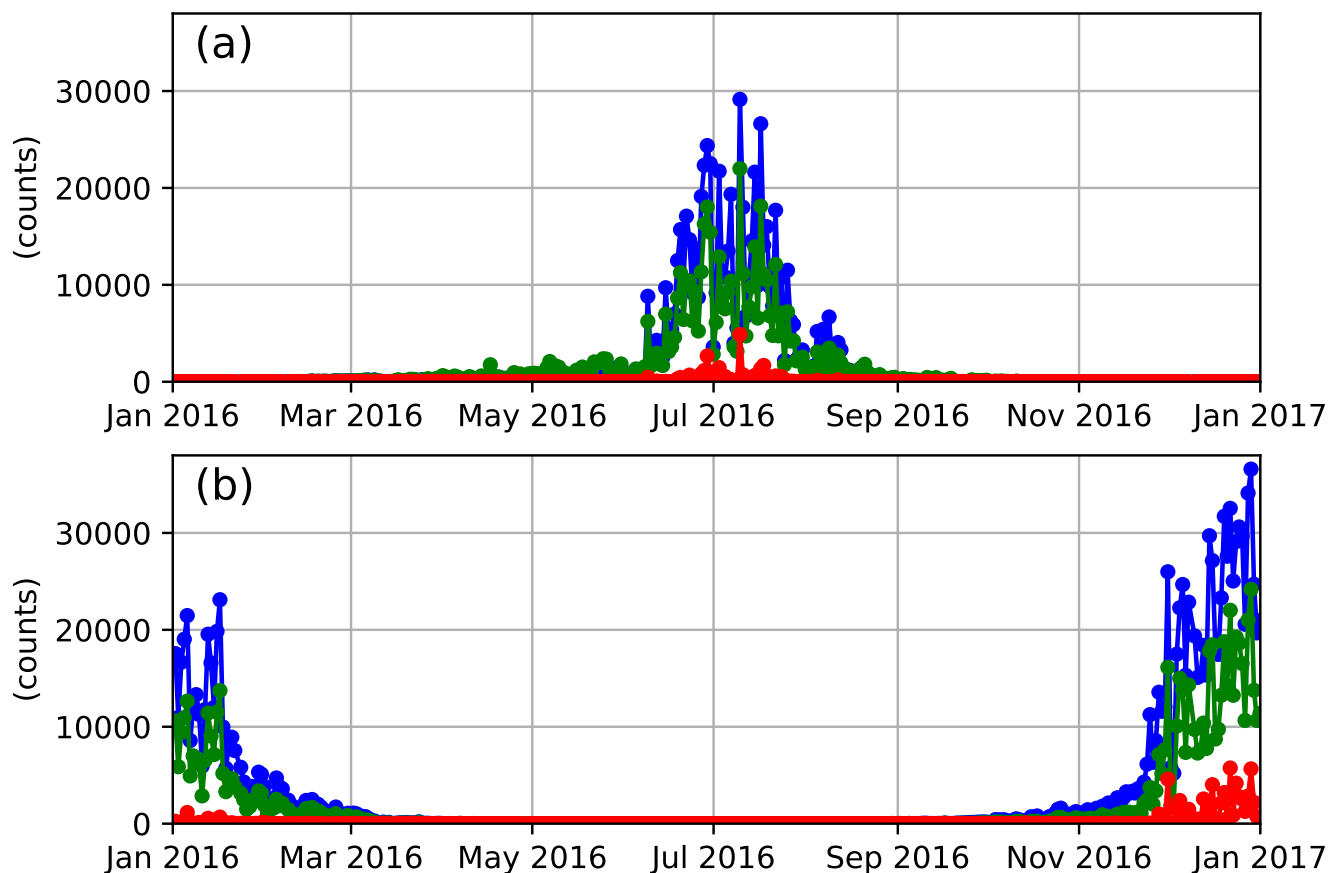


Figure 3. (a) Yearly variations of the total emission intensities in a region at heights of 70–90 km and latitudes of 60–90°N in 2016. Blue, green, and red lines correspond to the 3 visible bands, blue, green, and red bands, respectively. It should be noted that the upper limit of the latitude range is actually $\sim 81^\circ$, that is the highest latitude of the tangential points when we set the height range of 70–90 km. (b) Same as Figure 3a, but those in a region at heights of 70–90 km and latitudes of 60–90°S.